

## Turbulent Vortex Shedding across Internal Structure in Thermoacoustic Oscillatory Flow

Open  
Access

Siti Hajar Adni Mustaffa<sup>1</sup>, Fatimah Al Zahrah Mohd Saat<sup>1,2,\*</sup>, Ernie Mattokit<sup>1,2</sup>

<sup>1</sup> Fakulti Kejuruteraan Mekanikal, Universiti Teknikal Malaysia Melaka, Hang Tuah Jaya, 76100, Durian Tunggal, Melaka, Malaysia

<sup>2</sup> Centre for Advanced Research on Energy, Universiti Teknikal Malaysia Melaka, Hang Tuah Jaya, 76100, Durian Tunggal, Melaka, Malaysia

### ARTICLE INFO

### ABSTRACT

#### Article history:

Received 12 January 2018

Received in revised form 17 March 2018

Accepted 24 April 2018

Available online 14 June 2018

A knowledge about vortex shedding frequency is important in order to understand the vortex shedding flow phenomena using the associated dimensionless parameter known as the Strouhal number. This paper presents the results of numerical simulations of vortex shedding processes at the end of a stack of parallel-plates, due to an oscillating flow induced by an acoustic standing wave (thermoacoustic case). The oscillating flow is simulated using Reynolds-averaged Navier-Stokes (RANS) turbulence models which are four-equation Transition SST and two-equation SST  $k-\omega$ . Three drive ratios, DR (defined as the ratio of maximum pressure amplitude to the mean pressure) of 0.45%, 0.83% and 1.0% are investigated. The models were simulated at two flow frequencies which are 13.1 Hz and 23.1 Hz. The vortex shedding frequency was analysed after simulation reached a steady oscillatory flow condition. Two and four vortices flow phenomena were observed for both frequencies as drive ratio increased up to 1.0%. The Strouhal number has been obtained based on the vortex shedding frequency. The results show that vortex shedding pattern appears more stable at all the three drive ratios as the flow frequency increases.

#### Keywords:

Turbulent vortex shedding, oscillatory flow, thermoacoustics

Copyright © 2018 PENERBIT AKADEMIABARU - All rights reserved

## 1. Introduction

Vortex shedding flow phenomena can be seen in various engineering field such as wind engineering and industrial aerodynamics [1], engineering design [2], ocean engineering [3] and fluids and structures [4]. The alternate formation and shedding of vortices creates alternate forces which occur more frequently as the velocity of the flow increases. Vortex shedding phenomena is representing the dynamics of fluid as it flows over certain object. Vortices are rotational movement of the flow that occurs at certain frequency. Vortices developed around the object can bring harm on the object if it appears at the resonance frequency of the object. This may become important in the design of a buildings.

One of the examples is the world tallest buildings which is Burj Khalifa, in Dubai, UAE, where a group of engineers incorporates a variation in cross-section with height to ensure that vortices are

\* Corresponding author.

E-mail address: [fatimah@utem.edu.my](mailto:fatimah@utem.edu.my) (Fatimah Al Zahrah Mohd Saat)

not shed coherently along the entire height of the building [2]. This is also to avoid the possible danger of “resonance” on the structure. Resonance is a phenomenon when a system is driven at a vortex shedding frequency similar to the natural frequency of the system [5]. One dramatic example of the danger of ‘resonance’ was the collapse of the Tacoma Narrows Bridge in 1940 [6]. Evidently, at large scale, vortex shedding can be very dangerous. In essence, the vortex shedding alters the fluid dynamics of flow even if the phenomenon appears at low scale. The impact can be seen especially in the distribution of energy within energy related devices. Vortex shedding phenomena may lead to the lost or gain of energy in the system.

In general, vortex shedding occurs when a fluid flows past a bluff body and then be separated from the surface of the structure to form vortices (normally seen as wake) at the rear of the bluff bodies. Past investigation reported that the vortices might lead to one- or two-shear layers instability [7]. At relatively low speeds, the spiral vortices are created periodically and symmetrically from both sides of the body. However, at higher fluid speeds, the vortices are shed alternatively; on one side of the body first and then on the other side of the body later. This phenomenon has also attracted the interest of researchers in thermoacoustics field of study. In thermoacoustic systems (engines or refrigerator), the thermodynamic processes inside the system are normally referred to as the ‘thermoacoustic effect’. The ‘thermoacoustic effect’ often happened at high amplitude acoustic excitation when oscillatory flows of fluid interacts with the surfaces of internal structures (i.e. stack/regenerator or heat exchanger) so that heat transfer mechanisms and thermodynamics processes take place [8]. The internal structures known as ‘stack’ (mainly consist of parallel-plates used in standing-wave thermoacoustic systems) is the medium where the interaction between oscillatory flow and solid surface of object happens. In oscillatory flow, the fluid flow changes direction over time following the cyclic nature of the flow. Hence, vortex tends to appear at both ends of the structure depending on the direction of flow.

The characteristic of flow in thermoacoustics is commonly represented by a term known as drive ratio, DR. Drive ratio, DR, is used to represent the intensity of the acoustic standing wave inside the resonator. The vortex shedding phenomena in oscillatory flow is usually dominated by concentrated vortices that shed from the plate ends and then returns back into the channel between the plates as the flow reverses. This leads to potentially an additional disturbance in the flow of fluid within the structure. This process might affect the performance of the thermoacoustic systems. Previous numerical study reported that turbulence might appear at very low Reynolds number [9]. Yet, the investigation of turbulence in low Reynolds number in thermoacoustic applications is still lacking. Recent study [10] visualized the vortex shedding processes for high Reynolds number, up until  $Re = 3968$ , as the fluid flows out of the stack by using Particle Image Velocimetry (PIV) technique. The data were represented using the non-dimensional parameter known as Strouhal numbers,  $St$ , defined as  $St = fd/U$  where  $f$  is a vortex shedding frequency,  $d$  is the characteristic dimension (e.g. cylindrical diameter) and  $U$  is the free stream velocity, respectively. It was summarised that (a) at  $Re = 2947$ , the vortex patterns over the ejection stage change from attached symmetrical vortices from both sides of the plates to alternate shedding, (b) at  $Re = 3573$ , the alternate vortex shedding dominate in the ejection stage and (c) at  $Re = 3968$ , the vortex patterns of the alternate shedding evolve into elongated vortex structures in the deceleration stage. In order to study the vortex structures at the end of the stack plates, the vorticity,  $\omega_z$ , was calculated using two-dimensional representation defined as,

$$\omega_z = \frac{dv}{dx} - \frac{du}{dy} \quad (1)$$

It is noteworthy that, in normal unidirectional flow over objects, the critical Reynolds number usually exceeds 2000. In oscillatory flow, the fluid flows in two directions (bidirectional). Turbulence in oscillatory flow was found at the critical Reynolds number of 400 [11]. The Reynolds number in [11] was defined as  $Re_{crit} = 2\hat{u}/(v\omega)^{1/2}$ , where  $v$  = kinematic viscosity,  $\omega$  = frequency (radian) and  $\hat{u}$  = axial velocity amplitude. As the flow oscillates back and forth across objects, turbulence behaviour tends to appear early. Instability of the flow in oscillating type movements is difficult to understand and therefore not well defined. Previous investigation reported that early-stage turbulence was detected at Reynolds number as low as 100 [9]. The early stage of turbulent was expected to be the results of forward and backward movements of fluid across object. Numerical studies of the above phenomena within the thermoacoustic systems are relatively limited. Past study investigated the oscillating flow of thermoacoustic system involving thin ( $d = 0.15\text{mm}$ ) and thick ( $d = 1.0\text{ mm}$ ) stack plates [10]. In thick-plate configurations, they clarified the presence of concentrated vortices near the edge of the plate with different signs of vorticity. The concentrated vortices were also found occurring inside the channel and in the open region outside the channel. However, the formation of the defined eddies was not seen in thin-plate configuration. In most cases, the vorticity distribution in the wake exhibits the presence of elongated layers that extend well outside the channel. Still, studies related to vortex shedding phenomena and their impact on thermoacoustic performance are still very limited. Following the discovery of the early-stage turbulence for oscillatory flow at low Reynolds number [9], the current work has been conducted to investigate the vortex shedding processes at low Reynolds numbers ( $300 < Re_d < 900$ ) and the associated shedding frequency in oscillatory flow conditions.

## 2. Methodology

In the present work, a two-dimensional (2D) computational domain is developed using ANSYS FLUENT based on the experimental rig developed at Universiti Teknikal Malaysia Melaka [12]. The computational domain, as shown in Figure 1, consist of a structure known as 'stack'. In Figure 1, this structure is shown as the parallel-plates arrangement that is placed at the middle of the computational domain. The computational domain was built to cover a length of 300 mm to the left and right sides of the 'stack'. The 'stack' is made of sixteen aluminium plates of 3 mm thick ( $d$ ), 200 mm long ( $l$ ) and with gap spacing ( $D$ ) of 6 mm between each plates. This arrangement leads to the porosity of 66.76%. The porosity is defined as the ratio of space occupied by air over the total area of the space.

In this study, the variation of flow pattern is investigated at two different flow frequencies of 13.1 Hz and 23.1 Hz. The stack is placed at a location of 0.17 of the wavelength. At flow frequency of 13.1 Hz, the stack is located about 4.5 m from the location of pressure antinode, while at flow frequency of 23.1 Hz, the location of stack is 2.6 m from the pressure antinode. The pressure antinode is a location where pressure amplitude of the acoustic wave is at maximum value [12]. The parallel-plates stack geometry was chosen for this study because of its simplicity in both maintenance and fabrication.

The model has been checked for grid independency and it was found that flow was not affected by grid size when the model with 59880 cell counts was used. Data are processed after steady oscillatory flow condition is achieved (i.e. oscillating pressure and velocity are not changing with oscillation cycle). The data was taken at two locations; (i) at the middle of the stack (labelled as 'm'), (ii) at the end of the stack (labelled as 'e') as shown in Figure 1.

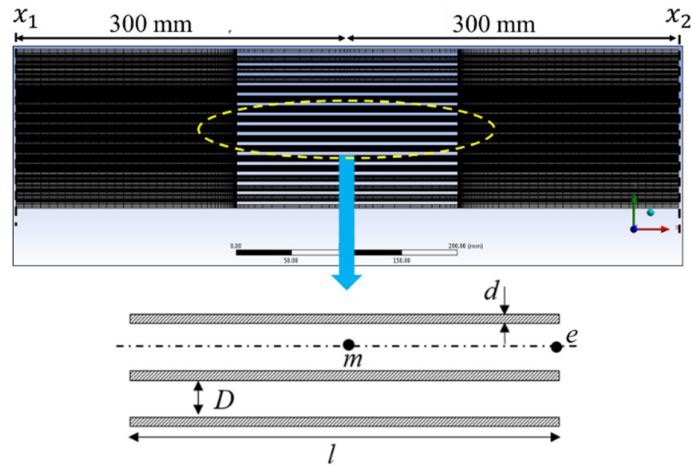


**Fig. 1.** Schematic diagram of computational domain; (top) meshing, (bottom) enlarge view of geometry of the stack (only three stack of plates shown)

Oscillating pressure,  $P_1$ , is placed at location  $x_1$  and oscillating mass flux,  $m'_2$ , was placed at location  $x_2$ , as shown in Figure 1. Pressure and velocity are set to be  $90^\circ$  out of phase following the requirement for standing-wave thermoacoustics system. The mean pressure was set to 0.1 MPa. The unsteady models were solved using a time-step size of  $1/1200f$  and the solution was monitored to converge at every time step. The unsteady model was solved using a pressure-based solver with the application of Pressure-Implicit with Splitting Operators (PISO) scheme for the pressure-velocity coupling. The solver was chosen because it provides faster convergence for unsteady flow cases. Table 1 shows the boundary conditions for all the models in this study. Flow field simulations were performed for 20 phases in one acoustic cycle as illustrated in Figure 2.

**Table 1**

Boundary conditions

Flow frequency, $f$ (Hz)	Drive ratio, DR (%)	Oscillating pressure, $P_1$ (Pa)	Oscillating mass flux, $m'_2$
13.1	0.45	243.46	1.1828
	0.83	449.06	2.1815
	1.0	541.03	2.6284
23.1	0.45	256.31	1.2198
	0.83	472.74	2.2499
	1.0	569.57	2.7108

Additional parameters which are turbulent intensity,  $I = 0.16(Re)^{-1/8}$ , calculated using Reynolds number,  $Re = \rho UD/\nu$  and turbulent length scale,  $\ell = 0.07D$  was assigned at both inlet and outlet boundaries. The Reynolds number was calculated using velocity,  $U$ , obtained from theoretical calculation at locations  $x_1$  and  $x_2$  for both flow frequencies. The terms  $\rho$  and  $\nu$  represent density and viscosity respectively. The boundary conditions were calculated based on the values obtained from lossless equations of quarter-wavelength device [9].

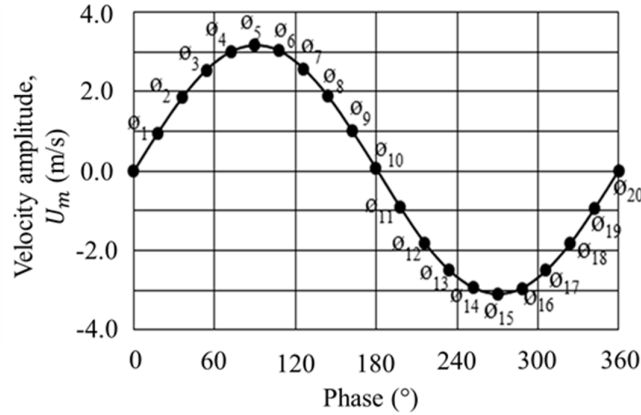


**Fig. 2.** Phase-averaged velocity at the middle of the stack for 20 phases of a flow cycle

### 3. Results and Discussion

#### 3.1 Validation and Verification

The velocity amplitude at point ‘m’, as shown in Figure 1, is obtained for the purpose of model validation. The results are shown in Figure 3. The model is validated by comparing the numerical results to the published data and theoretical data. The results of the drive ratios of 0.45%, 0.83% and 1% in the current study has been obtained using four-equation Transition SST and two-equation Shear-Stress Transport (SST)  $k-\omega$  turbulence models.

Figure 3 shows the results of current study compared to the results from theoretical equations [8], experimental findings of [13] and [9]. It is worth mentioning here that the theoretical equations was derived for laminar flow. It is found that the results of current study are slightly lower than experimental findings of [9] and [13]. As expected, theoretical equation under-predicts the value of velocity for all investigated drive ratios. This may be due to the appearance of turbulence as reported in [9]. Consistent with results of others, the values of velocity amplitude at point ‘m’ from CFD models of current study are also higher than the theoretical estimation but the differences are not as big as reported in other published works. Deviation from laminar model is only seen at drive ratio of 1%. This could be related to the behavior of fully developed flow due to the long plates involved in current study.

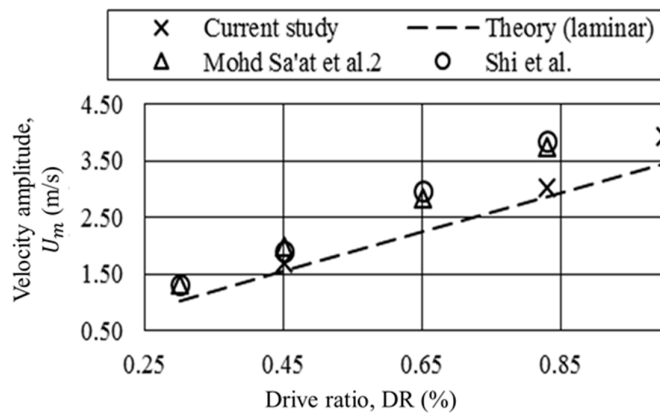


**Fig. 3.** Validation of velocity amplitude for model with flow frequency of 13.1 Hz

Unfortunately, perfect comparison may not be made at this point because the experimental design of plates used in [9] and [13] are not exactly the same as plates used in this study. However, the flow conditions in [9] and [13] are exactly the same as the condition used in the current model. The only difference is the length of plates. Nonetheless, Figure 3 confirms that the values from current CFD models are within values reported in published works.

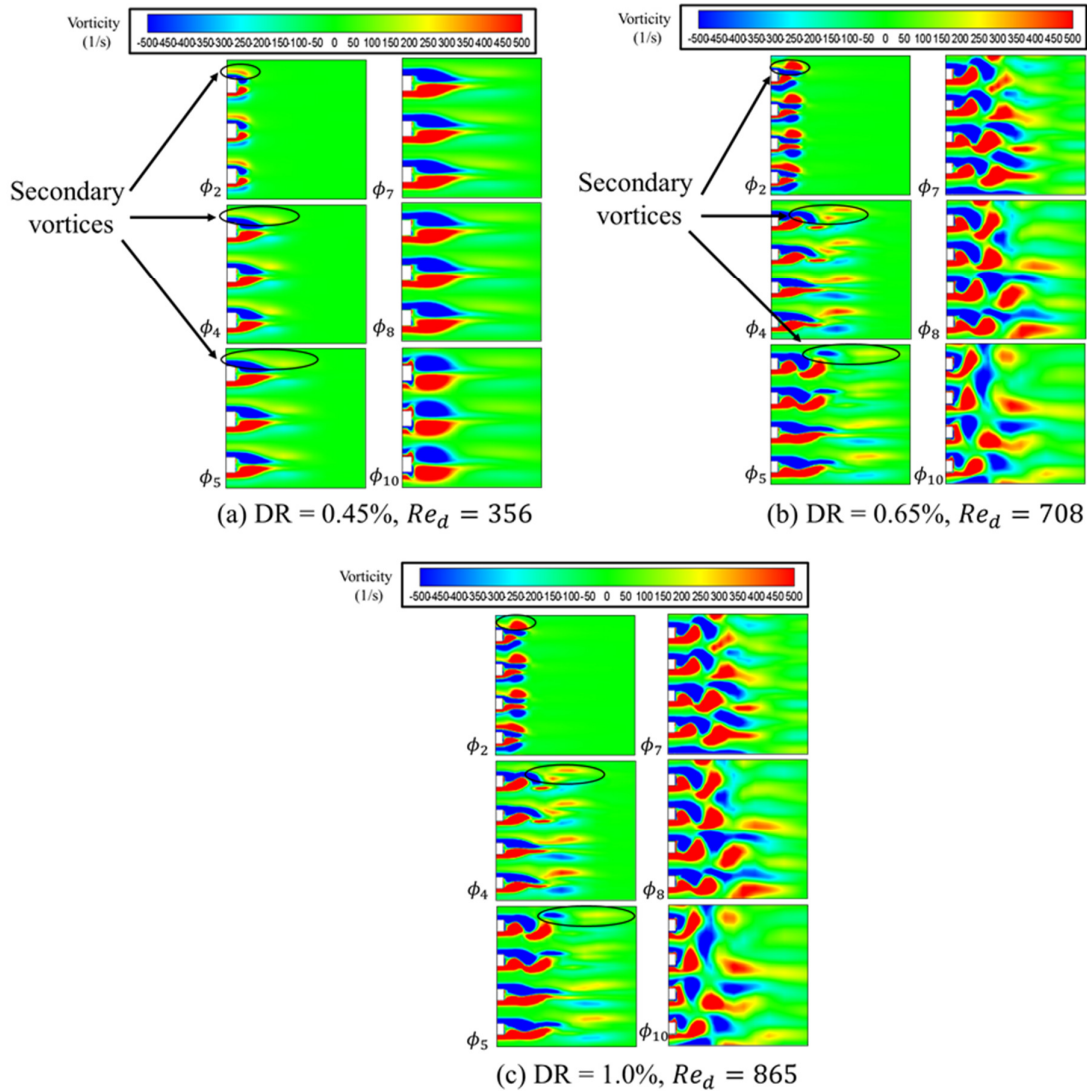
### 3.2 Flow Visualization Results

The vortex shedding phenomenon at the end of the stack plates in oscillatory flow conditions have been visualized by Shi *et al.*, [15] using Particle Image Velocimetry (PIV) method. They found that shedding vortices appeared at the end of plates during ejection stage and the flow patterns turned out to be similar to the classical von Karman “vortex street” pattern where the elongated vortex structures break up into a series of more discrete vortices. This paper presents vortex shedding patterns for two tested flow frequencies of 13.1 Hz and 23.1 Hz. As illustrated in Figure 2, the first part of the flow cycle is represented by phases of  $\phi_1$ - $\phi_{10}$  and the second part of the flow cycle is represented by phases of  $\phi_{11}$ - $\phi_{20}$ . The results shown in Figure 4 and Figure 5 should be interpreted in the perspective of oscillatory flow. In oscillatory flow, fluid flows forward during the first part of the cycle, while fluid reverses during the second part of the cycle. In this paper, the results are only shown for selected six phases which are  $\phi_2$ ,  $\phi_4$ ,  $\phi_5$ ,  $\phi_7$ ,  $\phi_8$  and  $\phi_{10}$  as presented in Figure 4 and Figure 5. Table 2 shows velocity amplitude at point ‘*m*’, as shown in Figure 1, for two investigated turbulence models.

**Table 2**  
 Comparison of velocity amplitude at point ‘*m*’ between numerical models

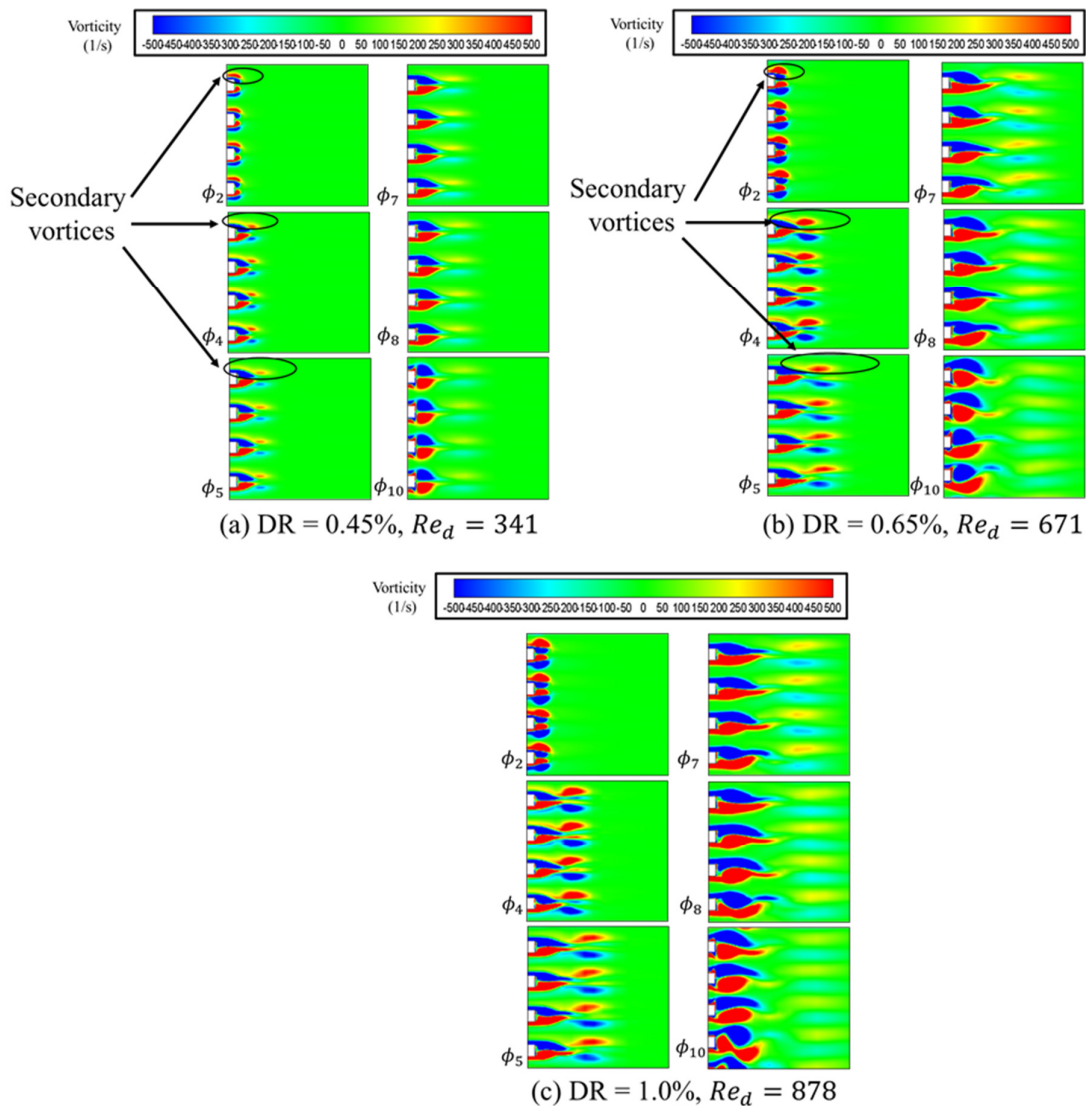
Flow frequency, <i>f</i> (Hz)	Drive ratio, DR (%)	$U_m$ (m/s)	
		CFD_Transition SST	CFD_SST k- $\omega$
13.1	0.45	1.70	1.70
	0.83	3.13	3.13
	1.0	3.74	3.90
23.1	0.45	1.65	1.66
	0.83	3.06	3.09
	1.0	3.67	3.74

Figure 4 presents the vorticity contour for drive ratios of 0.45%, 0.83% and 1%. The flow was visualized using SST k- $\omega$  turbulence model. The vorticity contour in Figure 4 is for flow frequency of 13.1 Hz, while the vorticity contour in Figure 5 is for flow frequency of 23.1 Hz. Figure 4(a) shows vortex shedding at the end of the plates for DR = 0.45%. At the early stage in flow cycle, in phase  $\phi_2$ , as the flow starts to accelerate, a pair of main vortex structures (shown as dark blue and red) appear along with a pair of secondary layer of vortices as can be seen at the end of the plates. As the velocity gradually increases, as can be seen in phases  $\phi_4$  and  $\phi_5$ , the flow pattern changes in a way that the attached vortex structure becomes more elongated but still remain symmetrical relative to the centreline between the plates. However, at intermediate drive ratio, DR = 0.83%, at phase  $\phi_4$ , apart from the pair of attached vortex structures, the secondary appear more distinct compared to DR = 0.45%. As the flow start to wiggle, as shown in Figure 4(b)( $\phi_5$ ), the flow showed two significant flow phenomena which are two vortices of opposite sign (a dipole) and four vortices are formed behind each plates, as reported in Aben *et al.*, [7]. The flow is distorted as it experiences a reverse situation. In Figure 4(c), with reference to phases  $\phi_8$  and  $\phi_{10}$ , the flow seems like a “vortex street” pattern but it is not exactly the “vortex street” as observed in high speed unidirectional flow.



**Fig. 4.** Vorticity contour for drive ratios, (a) DR = 0.45% ( $Re_d = 356$ ), (b) DR = 0.65% ( $Re_d = 708$ ) and (c) DR = 1% ( $Re_d = 865$ ) at flow frequency of 13.1 Hz

In the current situation, this pattern occurred due to the “breakage” of vortex structure as flow reverse. At high drive ratio, DR = 1% (corresponding to the high flow amplitude), as the velocity starts to increase to a maximum value, as represent in phase  $\phi_5$ , the vortex is shedding to a longer distance away from the plate compared to the previous drive ratios. This can be seen by comparing the results of phase  $\phi_4$  for all drive ratios studied in Figure 4. The four vortices flow phenomena is seen at the end of plates for all drive ratios. However, as the drive ratio increases the strength of vorticity becomes bigger and the feature of four vortices becomes more significant. Figure 5(a), (b) and (c) show the vorticity contour for drive ratios of 0.45%, 0.83% and 1% for flow frequency of 23.1 Hz.



**Fig. 5.** Vorticity contour for drive ratios, (a) DR = 0.45% ( $Re_d = 341$ ), (b) DR = 0.65% ( $Re_d = 671$ ) and (c) DR = 1% ( $Re_d = 874$ ) at flow frequency of 23.1 Hz

Comparison between results of flow visualization shown in Figure 4 and Figure 5 revealed two main differences; (i) as the flow frequency increase, the symmetrically main vortex (shown as dark blue and red contour) shed at the end of plates becomes shorter, (ii) the “vortex street”-like pattern is not prominent for the range of investigated drive ratios related to flow frequency of 23.1 Hz. This can be observed by comparing Figure 4(c) and Figure 5(c). The results in Figure 4 exhibit similar pattern as reported in [2]. This proved that the model is correct. Figure 5 shows new finding related to vortex patterns as the flow frequency increase.

### 3.3 Strouhal Number ( $St$ ) Results

In order to obtain further insight into various vortex shedding processes as described in Section 3.2, the Fast Fourier Transform algorithm is used to estimate the vortex shedding frequency at certain distance at the end of plates. Figure 6 shows the power spectrum between drive ratios at flow

frequencies of 13.1 Hz and 23.1 Hz. The graph is plotted in Matlab software by inserting the values of axial velocity obtained from simulation at each time-step size for several cycles. The peak frequency as can be observed in Figure 6 corresponds to the dominating vortex shedding frequency. The peak frequencies can be used to calculate the Strouhal number. Strouhal number represents a measure of ratio of the inertial forces due to the unsteadiness of the flow. Here the Strouhal number,  $St$ , is defined as  $St_d = \hat{f}d/U_e$  where  $\hat{f}$  is a vortex shedding frequency,  $d$  is the thickness of the plates and  $U_e$  is the velocity amplitude at the end of the stack plates as shown in Figure 1.

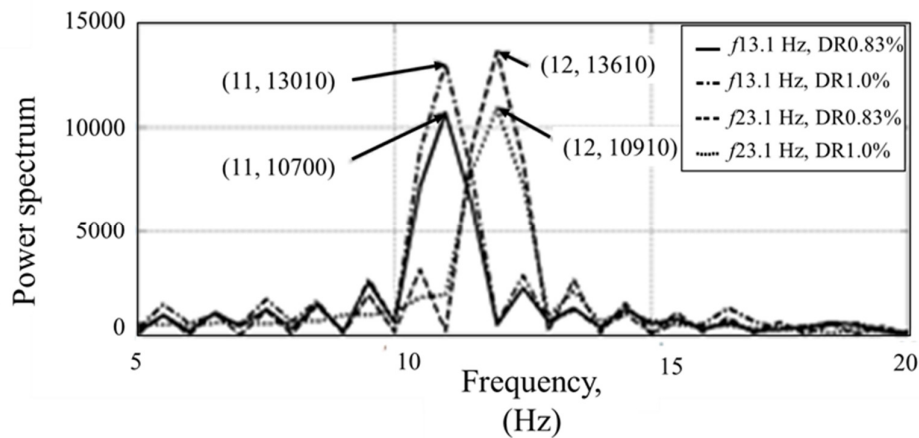


**Fig. 6.** Power spectrum of flow frequencies of 13. Hz and 23.1 Hz

Table 3 show the results of Strouhal number associated with Reynolds number for drive ratios of 0.83% and 1%. At each frequency, the Strouhal number drops as Reynolds number increase. As the flow frequency increases, the values of Strouhal number show slight increment. Unfortunately, the reason behind this phenomena is still unknown and a more detail investigation is needed to understand this behaviour.

**Table 3**

Variation of Strouhal number values associated with Reynolds number

Flow frequency, $f$ (Hz)	Drive ratio, DR (%)	Reynolds number, $Re_d$	Strouhal number, $St_d$
13.1	0.83	708	0.01025
	1.0	865	0.00840
23.1	0.83	671	0.01180
	1.0	818	0.00968

#### 4. Conclusion

This paper has demonstrated the vortex shedding phenomena occurring at the end of stack plates. The vortex shedding pattern for both flow frequencies can be categorized into two and four vortices flow phenomena. This is consistent with results from published works. However, the existence of secondary vortices found in this work need further investigation. The Strouhal number has been obtained based on the vortex shedding frequency. The results show that vortex shedding frequency,  $\hat{f}$ , behaves differently with the changes of flow frequency,  $f$ . Experimental works are needed to strengthen the findings reported in this paper. The experimental works is currently being conducted at UTeM.

## Acknowledgement

This work is jointly supported by Ministry of Higher Education Malaysia (FRGS/1/2015/TK03/FKM/03/F00274) and Universiti Teknikal Malaysia Melaka (UTeM).

## References

- [1] Pellegrino, Alberto, and Craig Meskell. "Vortex shedding from a wind turbine blade section at high angles of attack." *Journal of Wind Engineering and Industrial Aerodynamics* 121 (2013): 131-137.
- [2] Irwin, Peter A. "Vortices and tall buildings: A recipe for resonance." *Phys. Today* 63, no. 9 (2010): 68-69.
- [3] Mittal, H. V. R., Qasem M. Al-Mdallal, and Rajendra K. Ray. "Locked-on vortex shedding modes from a rotationally oscillating circular cylinder." *Ocean Engineering* 146 (2017): 324-338.
- [4] McClure, Jeffrey, and Serhiy Yarusevych. "Vortex shedding and structural loading characteristics of finned cylinders." *Journal of Fluids and Structures* 65 (2016): 138-154.
- [5] Woolfon, Michael M. "Resonance: Applications in Physical Science." (2015).
- [6] Bülh, K. Yusuf, and Robert H. Scanlan. "Resonance, Tacoma Narrows bridge failure, and undergraduate physics textbooks." *Am. J. Phys* 59 (1991): 2.
- [7] Matsumoto, M. "Vortex shedding of bluff bodies: a review." *Journal of Fluids and Structures* 13, no. 7-8 (1999): 791-811.
- [8] Swift, Greg W. "Thermoacoustics: A unifying perspective for some engines and refrigerators." (2003): 2379-2381.
- [9] MohdSaad, Fatimah AZ, and Artur J. Jaworski. "Numerical Predictions of Early Stage Turbulence in Oscillatory Flow across Parallel-Plate Heat Exchangers of a Thermoacoustic System." *Applied Sciences* 7, no. 7 (2017): 673.
- [10] Shi, Lei, Zhibin Yu, and Artur J. Jaworski. "Investigation into the Strouhal numbers associated with vortex shedding from parallel-plate thermoacoustic stacks in oscillatory flow conditions." *European Journal of Mechanics-B/Fluids* 30, no. 2 (2011): 206-217.
- [11] Merkli, P., and H. Thomann. "Transition to turbulence in oscillating pipe flow." *Journal of Fluid Mechanics* 68, no. 3 (1975): 567-576.
- [12] Mustafa, S. H. A., MohdSaad, F. A. Z., and Mat Tokit, E. "Design of experimental test-rig to investigate turbulence in oscillatory flow used in thermoacoustics." *Proceeding of Postgraduate Symposium on Green Engineering Technology* (2016).
- [13] Shi, Lei, Zhibin Yu, and Artur J. Jaworski. "Application of laser-based instrumentation for measurement of time-resolved temperature and velocity fields in the thermoacoustic system." *International Journal of Thermal Sciences* 49, no. 9 (2010): 1688-1701.
- [14] Aben, P. C. H., P. R. Bloemen, and J. C. H. Zeegers. "2-D PIV measurements of oscillatory flow around parallel plates." *Experiments in Fluids* 46, no. 4 (2009): 631-641.
- [15] Shi, Lei, Zhibin Yu, Artur J. Jaworski, and Abdulrahman S. Abduljalil. "Vortex shedding at the end of parallel-plate thermoacoustic stack in the oscillatory flow conditions." *World Academy of Science, Engineering and Technology* 49 (2009).